J. Phys.: Condens. Matter **2** (1990) 3093–3113. Printed in the UK

Universal diffusion-limited colloid aggregation

M Y Lin†‡‡, H M Lindsay‡, D A Weitz§, R Klein‖, R C Ball¶ and P Meakin††

† Department of Physics, Princeton University, Princeton, NJ 08544, USA
‡ Department of Physics, Emory University, Atlanta, GA 30322, USA
§ Exxon Research and Engineering Co, Rt 22E, Annandale, NJ 08801, USA
‖ Fakultat für Physik, Universität Konstanz, Konstanz, Federal Republic of Germany
¶ The Cavendish Laboratory, Madingley Road, Cambridge CB3 9HE, UK
†† E I DuPont de Nemours Co, Experimental Station, Wilmington, DE 19880-0356, USA

Received 4 September 1989, in final form 30 November 1989

Abstract. We study the process of diffusion-limited colloid aggregation (DLCA) using both static and dynamic light scattering. Static light scattering is used to measure the fractal dimension of the clusters as well as their structure factor, which is found to be in good agreement with that obtained from calculation using computer-generated clusters. Dynamic light scattering is used to probe both translational and rotational diffusion motion of the clusters. A method to separate their respective contributions is developed, allowing a quantitative determination of the average hydrodynamic radius. In addition, we determine the ratio of the hydrodynamic radius to the radius of gyration for individual aggregates, and find $\beta = 0.93$. A method is developed to scale all the dynamic light scattering data onto a single master curve, whose shape is sensitive to key features of the DLCA process. Good agreement is found between our prediction of the shape of the master curve and that obtained from experiments. Using several completely different colloids, we find that the shape of their master curves are identical, their fractal dimensions are identical and their aggregation kinetics are identical. This provides strong evidence of the universality of the DLCA regime of colloid aggregation.

1. Introduction

In recent years, there have been significant advances in our understanding of the process of colloid aggregation [1]. The key to these advances is the recognition that the highly disordered structure of colloidal aggregates can be quantitatively characterised by its scaling behaviour, and therefore is well described as a fractal. Furthermore, modern scaling concepts have found many applications in the description of the kinetics of aggregation processes.

The most widely considered form of colloid aggregation is that which begins with a suspension of monodisperse particles. Upon aggregation, these particles collide due to thier Brownian motion and stick together irreversibly to form rigid clusters. The clusters themselves continue to diffuse, collide and form yet larger clusters, resulting in a

‡‡ Present address: National Institute of Standards and Technology, React A106, Gaithersburg, MD 20899, USA.

0953-8984/90/133093 + 21 $03.50

polydisperse mass distribution. This process is called cluster–cluster aggregation, and is a non-equilibrium, kinetic growth process. Both the aggregation kinetics and the shape of the cluster mass distribution are intrinsically related to the structure of the clusters that are ultimately formed. A complete characterisation of this aggregation process must include a full description of both the structure of the clusters, as well as the shape and time evolution of the cluster mass distribution.

Two distinct, limiting regimes of colloid aggregation have been identified [2, 3]. They correspond directly to the regimes of rapid and slow aggregation that have been well established in the classical colloid literature [4]. The first of these regimes occurs when the aggregation rate is limited solely by the time between the collisions of the clusters due to their diffusion. This case is therefore called diffusion-limited cluster–cluster (colloid) aggregation (DLCA). The second limiting regime occurs when the reaction rate of two particles is much slower than the collision rate, so that a large number of collisions are required before two particles can stick together, resulting in a much slower aggregation rate. This case is called reaction-limited cluster–cluster (colloid) aggregation (RLCA).

An elegant and quite detailed picture of cluster–cluster aggregation has evolved in recent years [1, 5], based upon theoretical advances, extensive application of computer simulations and a variety of experimental measurements. Both regimes are found to have characteristic, yet distinct, behaviour. The cluster structure in both cases is fractal, with fractal dimension $d_f \simeq 1.8$ for DLCA and $d_f \simeq 2.1$ for RLCA. The cluster mass distribution in both cases exhibits dynamic scaling in that its shape remains constant in time. For DLCA, the distribution is relatively flat up to some characteristic mass M_c, falling exponentially above M_c. For RLCA, the distribution is power-law in shape up to M_c, with an exponential cut-off at higher masses. The characteristic mass grows linearly in time for DLCA and exponentially for RLCA.

Experimentally, both static and dynamic light scattering have been among the techniques most frequently used to probe these features. Static light scattering is used to probe the structure of the colloidal aggregates, and to measure their fractal dimension. Dynamic light scattering probes both translational and rotational diffusion of the clusters, and thus is used as a measure of the cluster size and the cluster anisotropy. Dynamic light scattering also serves as a probe of the aggregation kinetics and can be used to help determine the shape of the cluster mass distribution.

In this paper, we present a comprehensive study of the DLCA regime, utilising several different colloids. The relatively flat cluster mass distribution of the DLCA regime minimises the complications introduced by polydispersity in the analysis of light scattering results. By contrast, the effects of polydispersity significantly complicate the analysis of the data obtained from the RLCA regime, and these problems are discussed elsewhere [6]. Here, we develop a detailed description of both static and dynamic light scattering from DLCA clusters, based on the fractal structure of the colloidal aggregates and the shape of the cluster mass distribution. We discuss a method to determine accurately the characteristic hydrodynamic radius using dynamic light scattering for large clusters when both translational and rotational diffusion contribute. A series of calibration curves for different scattering angles are presented, enabling the two contributions to be disentangled and the true characteristic hydrodynamic radius of DLCA clusters to be determined from the experimentally measured value. Here, we use the calibration curves to follow the aggregation kinetics.

In this paper, we also compare the behaviour of several different colloids aggregated under diffusion-limited conditions. To do this, we develop a technique for scaling the

results of dynamic light scattering, obtained at different times and different scattering angles, onto a single master curve [7]. The shape of this master curve is sensitive to the key features of the aggregation process: the shape of the cluster mass distribution; the fractal dimension of the aggregates; the anisotropy of the aggregates; and the shape of the cluster structure factor. The scaling factors used in obtaining the master curves provide an alternative, sensitive and model-independent probe of the aggregation kinetics. Furthermore, those features specific to an individual colloid system, such as the particle radius, are scaled out of the master curve. Thus we can use the master curves to compare critically the aggregation of completely different colloids. In this paper, we compare the behaviour of three colloids, gold, silica and polystyrene latex, all aggregated under DLCA conditions. We show that the master curves for each of the colloids are identical. In addition, the fractal dimensions, measured by static light scattering, and the aggregation kinetics, measured by dynamic scattering, for each of the colloids are also identical. Thus, we conclude that DLCA is a unviersal regime of aggregation in the sense that it is independent of the specific chemical nature of the colloids [8].

The remainder of this paper is organized as follows. In section 2 we present a brief review of diffusion-limited colloid aggregation. This is followed in section 3 by a description of the details of the sample preparation and the light scattering experiments. We then discuss in section 4 experimental measurements of both static and dynamic light scattering, and present a self-consistent description of these results. In the following section (section 5) we develop a technique to separate the contributions of the translational and rotational diffusion to the dynamic light scattering and hence are able to extract a true hydrodynamic radius from the data. We are thus able to measure the aggregation kinetics. This is followed by section 6, in which we construct the master curve for a single colloid, and discuss the calculation of the expected shape. Finally, in section 7, we utilise static and dynamic light scattering and the master curves to compare critically the behaviour of the different colloids, and verify that DLCA is a universal process. A brief concluding section closes the paper.

2. Diffusion-limited colloid aggregation

A typical colloid aggregation process begins with a monodisperse solution of individual particles of radius a at a relatively low initial volume fraction $\varphi_0 \lesssim 10^{-4}$. The colloid is initially stable against aggregation due to a repulsive energy barrier E_b that exists between two approaching particles [3]. Diffusion-limited aggregation is initiated by reducing this energy barrier until it is much less than $k_B T$, ensuring that two particles stick immediately on collision. The energy of the bonds formed on aggregation are much greater than $k_B T$, so the aggregation process is completely irreversible, and the clusters formed are rigid. The clusters have a tenuous and highly disordered structure, which can be characterised as a fractal. Thus, if M denotes the mass of a cluster in units of the mass of the primary particles, and if R_g is the radius of gyration of the cluster, the relation

$$M = (R_g/a)^{d_f}$$

holds, where d_f is the fractal dimension. After the aggregation is initiated, a broad distribution of cluster masses evolves. The shape of this distribution remains constant in time, while the mass of the average or characteristic clusters grows with time. The structure of the aggregates, the shape of the cluster mass distribution and its time development are all interrelated. Therefore, a complete description of an aggregation

process requires a description of all these features. Here we briefly review the behaviour of these features for the DLCA regime.

Computer simulations [9, 10] have shown that the clusters formed under DLCA conditions are fractal, with $d_f \simeq 1.8$. The fractal dimension of such aggregates has been measured experimentally for several different colloids, including gold [11], silica [12] and polystyrene [13]. Several different techniques have been used, including the analysis of transmission electron micrographs (TEM), light scattering and x-ray scattering [14]. In all cases a value of $d_f \simeq 1.8 \pm 0.1$ is obtained, consistent with the computer simulation results.

The cluster mass distribution $N(M)$, which expresses the number of clusters of mass M, can be determined from the Smoluchowski rate equations. The solution exhibits dynamic scaling [15], and can be written as

$$N(M) = \bar{M}^{-2}\psi(M/\bar{M}) \tag{1}$$

where $\bar{M}$ is an average cluster mass, which can be defined as

$$\bar{M} = N_0/N_t \tag{2}$$

where $N_0 = \Sigma N(M)M$ is the total mass of the system and $N_t(t_a) = \Sigma N(M)$ denotes the total number of clusters at the elapsed time t_a from the initiation of the aggregation. The shape of the distribution, determined by the scaling function $\psi(x)$, is independent of time. The time dependence of the distribution is reflected in the moment of the distribution $\bar{M}$, and can be characterised by a dynamic exponent z, where $\bar{M} \sim t_a^z$. To a good approximation, the shape of the cluster mass distribution for DLCA is given by [16]

$$N(M) = \frac{N_0}{\bar{M}^2}\left(1 - \frac{1}{\bar{M}}\right)^{M-1}. \tag{3}$$

The shape of $N(M)$ as expressed by equation (3) is essentially independent of M up to $\bar{M}$, after which it decreases exponentially. Computer simulations of DLCA predict cluster mass distributions that are in good agreement with this result [17]. Experimentally, measurements using TEM counting of colloidal gold aggregates [18] and using electrical resistance counting of polystyrene latex aggregates [19] also support this result.

The time dependence of the characteristic cluster mass can also be determined by means of the Smoluchowski equations [16]. For DLCA, a linear dependence is predicted, so that $z = 1$ and

$$\bar{M} = t_a/t_0 + 1 \tag{4a}$$

where

$$t_0 = 3\eta V/(8k_B T N_0) \tag{4b}$$

with η the viscosity of the fluid and N_0/V the initial particle concentration. Computer simulations [17] also predict that $z = 1$. An experimental study of latex aggregates [19] found that the total number of clusters decreases as $N_t \sim t_a^{-1}$; thus $\bar{M} \sim N_t^{-1} \sim t_a$, resulting in $z = 1$, consistent with the theoretical predictions.

Diffusion-limited colloid aggregation is achieved when the repulsive barrier between two approaching particles of a stable colloid is reduced to an energy much less than $k_B T$, so that the rate of aggregation is limited solely by the time required for diffusion-induced collision between the clusters. This rate-limiting condition should, in principle, be achieved by any colloid system. If so, the characteristics of DLCA should pertain to the aggregation. In this sense, DLCA should be a universal regime of aggregation.

3. Experimental methods

In this paper, we study three colloids: gold, silica and polystyrene latex. Each is a charge-stabilised colloid. Each can be aggregated under either slow, RLCA or rapid, DLCA conditions.

The colloidal gold is made following a modification of a recipe due to Turkevich [20]. We heat 95 ml of a 5.3×10^{-5} M solution of sodium tetrachloroaurate ($NaAuCl_4$) at ~90 °C for at least 3 mins. To this, 5 ml of a 0.05% (by weight) solution of sodium citrate is added while stirring vigorously. The mixture is kept at 90 °C for 30 min while stirring constantly. During the first 10–15 min, the citrate reduces the gold, and the colloidal particles are formed, with the solution undergoing a series of changes in colour, finally attaining the characteristic wine-red colour. We find it necessary to keep the colloids at 90 °C for another 15–20 min to obtain an even distribution of the surface charges on the particles and to ensure reproducible results. The primary particles are reasonably spherical in shape and highly uniform in size. The average radius of the particles is 7.5 nm with an RMS deviation about the mean size [21] of roughly 10%. Assuming that all the gold is reduced, the concentration is about 1.7×10^{12} particles/cm^3 and volume fraction is $\varphi_0 = 2.8 \times 10^{-6}$.

Colloidal gold prepared in this way is very stable against aggregation because citrate ions, with a charge of -3, are adsorbed on the surface of the particles. The Debye–Hückel screening length of the solution as prepared is $\kappa^{-1} \sim 10$ nm, or roughly one particle radius. The surface potential of these gold colloids has been measured [21] to be ~25 mV, and we estimate that $E_b > 18k_BT$, making the colloid stable almost indefinitely. Aggregation is initiated by the addition of a neutral organic molecule, pyridine, which is preferentially adsorbed on the surface of the colloid, displacing the citrate ions and thereby reducing the surface charge and thus E_b. The particles can then stick to one another, forming metallic bonds. The amount of pyridine added determines whether the aggregation is diffusion- or reaction-limited. For DLCA, the final concentration used is 0.009 M. This is achieved by injecting 1 part of a 0.1 M pyridine solution into 10 parts of colloid, and immediately inverting the sample cell to mix the solutions. The initial aggregation proceeds very rapidly, as can be seen by the almost immediate change in colour of the solution, from the wine-red colour of the unaggregated particles to the blue colour of the small aggregates. After the initial mixing, the solution is not subjected to any mechanical disturbances, in order to eliminate any possible restructuring effects [22, 23].

The colloidal silica used is Ludox-TM, obtained from DuPont. It consists of particles with $a = 11$ nm and is diluted to $\varphi_0 = 1.7 \times 10^{-6}$ for the experiments. The colloid is initially stabilised by SiO^- groups on the surface of the particles. The pH is adjusted to pH $\geqslant$ 11 by addition of NaOH. The OH^- ions are necessary to catalyse the formation of the interparticle siloxane bonds. Aggregation is initiated by addition of NaCl, which decreases the Debye–Hückel screening length, reducing the repulsive barrier between the particles. Again a 1 to 10 dilution is used, with a final salt concentration of 1.7 M.

The polystyrene latex is also commercially available, and has $a = 19$ nm and is diluted to $\varphi_0 = 8 \times 10^{-7}$ for these experiments. The polystyrene is stabilised by charged carboxylic acid groups on the surface. Aggregation is initiated by adding 1 part of HCl solution to 10 parts colloid, to achieve to a final concentration of 1.2 M HCl. This both neutralises the surface charges and decreases the Debye–Hückel screening length. The interparticle bond of the aggregates are due to van der Waals interactions.

To achieve the limit of diffusion-limited aggregation requires that E_b be reduced to nearly zero. This demands considerable care in the preparation of each colloid and in

maintaining a sufficient degree of cleanliness in the glassware used. All the solutions prepared must be as clean and as free of impurities as possible. To clean the glassware and sample cells, we use a Chromerge soak for over 1 h, followed by a rinse in a dilute HCl solution and then a wash with copious amounts of water. Distilled, deionised and filtered water is used in every step. However, we find it crucial to filter only the water, and not the colloids, as the filtration process changes the colloid concentration and induces aggregation by changing the particle surface chemistry. These effects become increasingly problematic as the colloid is diluted with water to decrease φ_0. Dilution reduces the ratio of particle surface area to volume of solution, making the surface more susceptible to impurities. The colloidal gold seems particularly susceptible to these effects, as it exhibits an aging effect whereby its properties change if the colloid is more than a few days old. This problem was avoided by using a freshly prepared sample for each experiment.

For all colloids, the result of impurities either on the glassware, or in any of the solutions, is to preclude achieving a true diffusion-limited aggregation process. The impurities presumably adsorb on the colloid surface, preventing the complete reduction of E_b, reducing the initial aggregation rate to less than the DLCA limit. While this results in only a slight change in the measured aggregation kinetics, the fractal dimension of the resultant clusters is increased appreciably, consistent with aggregation in the intermediate regime [3], which begins as RLCA, but then crosses over to DLCA as the cluster concentration decreases and diffusion becomes dominant in limiting the aggregation rate. In fact, we find that monitoring d_f by static light scattering is an excellent method of ensuring the cleanliness of the glassware and solutions. A measured $d_f \sim 1.85$ indicates that the aggregation is truly DLCA, while an increase in the measured d_f to greater than ~ 1.95 invariably indicates problems with impurities. Our observations concerning the importance of using freshly prepared samples of colloidal gold, and avoiding the problems with changing the surface chemistry, introduced by filtration, are consistent with a report by Olivier and Sorenson [24]. They studied the aggregation of colloidal gold initiated by HCl. They used samples that were several months old, and were filtered immediately prior to use, and they were unable to achieve the limiting case of DLCA.

We use both static and dynamic (or quasi-elastic) light scattering. Static light scattering measures the time-averaged scattering intensity from the sample, $I(q)$, as a function of the scattering wavevector $q = (4\pi n/\lambda)\sin(\theta/2)$, where λ is the incident wavelength *in vacuuo*, n is the index of refraction of the water and θ is the scattering angle. Dynamic light scattering, by contrast, measures the temporal autocorrelation function of the scattering intensity [25],

$$G_2(t) = \langle I(t)I(0)\rangle \tag{5}$$

where t is the delay time and the angle brackets represent an ensemble average.

The detection optics are mounted on the rotating arm of a goniometer, allowing us to measure both the static and the dynamic scattering concurrently as a function of the scattering angle θ, and hence the scattering wavevector q. Our source is an argon-ion laser with a wavelength $\lambda = 488$ nm. For the colloidal gold samples, which strongly absorb the light, the incident intensity is maintained at less than 1 mW before entering the sample cell to avoid spurious heating effects. A 272-channel correlator is used to measure both the intensity autocorrelation function $G_2(t)$ and the average intensity $I(q)$. The sample time of the correlator is adjusted so that the magnitude of the autocorrelation function decays by about one decade for each measurement. The baseline B of the autocorrelation function is determined both from the measured average intensity and

from the correlator baseline channels, which are delayed an additional 1024 sample times. While the two methods usually agree to within 0.5%, the average intensity is always used in the analysis. Although we experimentally measure the intensity autocorrelation function, it is much simpler theoretically to calculate the normalised field autocorrelation function,

$$g_1(t) = \frac{\langle E^*(t)E(0)\rangle}{\langle E^*(0)E(0)\rangle}$$

where $E(t)$ is the scattered electric field. However, for fractal clusters the two are related [26] by the Siegert relationship [27]

$$G_2(t) = A'Bg_1^2(t) + B \tag{6}$$

where A' is a constant of the order of unity, which depends on the geometry of the detection optics. Much of our analysis is in terms of the initial time dependence of the autocorrelation function, as determined by the logarithmic slope at $t = 0$, or the first cumulant

$$\Gamma_1 = -[\partial \ln g_1(t)/\partial t]|_{t\to 0}. \tag{7}$$

To determine Γ_1, we fit the logarithm of the autocorrelation function to a third-order polynomial,

$$\ln g_1(t) = 1 - \Gamma_1 t + \tfrac{1}{2}\Gamma_2 t^2 - \tfrac{1}{6}\Gamma_3 t^3. \tag{8}$$

We find empirically that this fitting procedure gives a good approximation to the initial slope.

The measurements are performed in two ways. To obtain good statistics at large t requires averaging for long times. However, these averaging times must still be small on the timescale of the change in $\bar{M}$. This is difficult to achieve in DLCA since the aggregation rate is so rapid. Thus to obtain data at large t, we stop the aggregation at fixed time t_a, by adding a small amount of surfactant. We use sodium dodecyl-*o*-xylenesulphonate [28] at a concentration of 10^{-3} M. The surfactant adsorbs on the surface of the colloid particles, providing a steric stabilisation and thus halting further aggregation. However, since the amount of adsorbed surfactant is so small, neither the static nor the dynamic light scattering is modified. This method allows us to collect good-quality data at long delay times t and at several different values of q with a fixed $\bar{M}$. To assure good statistics, we average at least 10^6 times the longest correlation time t. However, the method is suitable only for colloidal gold, as we have been unable to find a surfactant with the required properties for the other colloids.

The second method is used for the other colloids. Here we repeatedly measure the autocorrelation function at different angles as the aggregation proceeds. However, since $\bar{M}$ is constantly changing we are able to collect data at each point for a shorter period of time. This limits the statistics of the data at larger delay times. Nevertheless, we are still able to determine Γ_1 with good precision.

4. Light scattering from colloidal aggregates

In this section, we develop a consistent description of both static and dynamic light scattering using a single sample for which the aggregation has been stopped at a time t_a.

We show that the static light scattering can be described using the structure factor determined from computer-generated DLCA clusters and the cluster mass distribution determined from the Smoluchowski equation, given by equation (3). This provides a measure of the average cluster mass of the distribution, $\bar{M}$. In addition, we are able to describe accurately the full shape of the correlation function measured by dynamic light scattering at several different values of q. To do so we use the same cluster mass distribution, the same structure factor for the clusters and the same value of $\bar{M}$ determined from the static light scattering. However, in addition, we must include the effects of rotational diffusion, which become increasingly important as q increases. Furthermore, by comparing the static and dynamic scattering data at low q, we are able to determine β, the ratio of the hydrodynamic radius R_h to the radius of gyration R_g of the individual clusters. Since we must stop the aggregation, we use colloidal gold for these measurements.

The static scattering intensity $I_M(q)$ of clusters of mass M is proportional to the Fourier transform of the pair density correlation function of such clusters. Therefore, a measure of the q dependence of the scattering intensity reveals the structural properties of the clusters and, consequently, can determine the fractal dimension. However, since the clusters are polydisperse, the measured scattering intensity $I(q)$ is an average of $I_M(q)$ over the cluster mass distribution. Therefore, $I(q)$ can be written as

$$I(q) = \sum_M N(M) I_M(q) \tag{9}$$

where

$$I_M(q) = AM^2 S(qR_g). \tag{10}$$

Here A is a constant depending on the experimental conditions and the scattering cross section of the individual particles. We denote by $S(qR_g)$ the static structure factor of clusters of mass M, having a radius of gyration $R_g = aM^{1/d_f}$. The structure factor depends on q and R_g through the dimensionless combination qR_g [22], since R_g is the only relevant length scale of a self-similar cluster. Its limiting behaviour is

$$S(qR_g) = \begin{cases} 1 & \text{for } qR_g \ll 1 \\ (qR_g)^{-d_f} & \text{for } qR_g \gg 1. \end{cases} \tag{11}$$

For $qR_g \simeq 1$, the shape of $S(qR_g)$ is determined by the form of the cut-off of the pair density correlation function introduced by the finite size of the clusters. It follows from equations (9) to (11) that the total scattering $I(q)$ also has the same form of limiting behaviour as $S(qR_g)$: at sufficiently low q it is isotropic, independent of q, while at sufficiently large q it also exhibits the q^{-d_f} behaviour characteristic of the fractal structure. However, the polydispersity in the cluster mass distribution smears the cross-over between these two limiting regions so it extends over a larger range of q. Here we choose a sample for which the aggregation is stopped when the cross-over region can be probed by the experimentally accessible scattering wavevectors. The data are shown by the points in figure 1.

The data are described with equations (9) and (10). For the cluster mass distribution we use the DLCA form in equation (3). For the structure factor, we use

$$S(x) = (1 + C_1x^2 + C_2x^4 + C_3x^6 + C_4x^8)^{-d_f/8} \tag{12}$$

where $x = qR_g$, $C_1 = 8/3d_f$, and $C_2 = 2.50$, $C_3 = -1.52$ and $C_4 = 1.02$. The values of

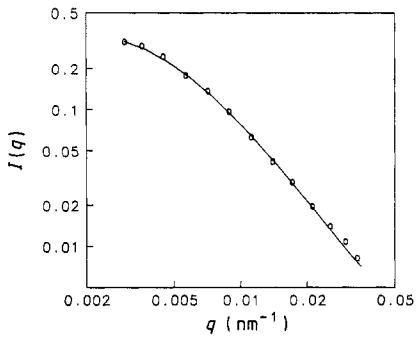

Figure 1. Static light scattering intensity from colloidal gold aggregates formed by DLCA. The data were taken when the sizes of the aggregates were not large enough for the intensity to exhibit a linear fractal scaling in the logarithmic plot. The full curve is a calculation using equations (3), (9), (10) and (12). An average cluster mass of $\bar{M} = 165$ is obtained from the fit.

the coefficients are obtained by fitting the expression in equation (12) to the $S(qR_g)$ calculated directly using computer-generated DLCA clusters. A detailed study [22] of the static light scattering from both DLCA and RLCA clusters shows that the form of the structure factor in equation (12) provides a much better description of the finite extent of the fractal aggregates than other forms of $S(qR_g)$ suggested in the literature. The value of $\bar{M} = 165$ is obtained from a fit to the data, shown by the full curve in figure 1. As can be seen, the agreement is excellent.

To analyse the dynamic light scattering data from this sample, we must consider the effects of both translational and rotational diffusion [23, 26], since, at large angles, many clusters in the distribution are larger than q^{-1}. The autocorrelation function $g_1(t)$ of the field scattered from an anisotropic, inhomogeneous object can be calculated under the assumption that the effects of the coupling of translational and rotational diffusion are negligible. Both computer-generated and experimentally produced DLCA clusters have typical overall aspects ratios of about 2, so this assumption applies. Then, the field autocorrelation function can be expressed as [23]

$$g_1(t) = \frac{1}{I(q)} \sum_M N(M)M^2 \exp(-q^2Dt) \sum_{l=0}^{\infty} S_l(qR_g) \exp[-l(l+1)\Theta t]. \tag{13}$$

Here, $D = \zeta/R_h$ is the translational diffusion coefficient and $\Theta = \frac{3}{4}\zeta/R_h^3$ is the rotational diffusion coefficient of a cluster of mass M, and $\zeta = k_BT/6\pi\eta$. Each term in the second sum, which represents the rotational contribution, is weighted by a factor $S_l(qR_g)$. These factors are essentially the multipoles of the structure factor, since $S(qR_g) = \Sigma_l S_l(qR_g)$. They reflect the anisotropies of the geometric structure of the clusters, expressed in Fourier space.

From equation (13) we see that translational and rotational diffusion contribute to the autocorrelation function with different decay rates. For translational diffusion, the decay rate is $\Gamma_t = Dq^2$, and is proportional to q^2. By contrast, the lth term in the sum originating from rotational diffusion has a decay rate $\Gamma_l = l(l+1)\Theta$, independent of q. The q dependence due to rotations is caused by the anisotropy of the structure, and thus is reflected in the components $S_l(qR_g)$ of the structure factor.

The complete set of multipoles, $S_l(qR_g)$, can be calculated with computer-generated DLCA clusters, and used in equation (13) to determine the autocorrelation function. The results obtained by this technique are in excellent accord with experimental measurements [26]. However, this method is computationally intensive, making it relatively inflexible and difficult to apply to clusters larger than $M \simeq 1000$ and $qR_g > 10$. To extend

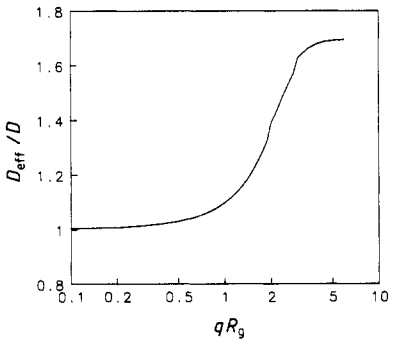

Figure 2. The scaled effective diffusion coefficient, including the effects of rotational diffusion for DLCA clusters. It is an average of calculations from nearly 200 computer-generated clusters of different masses.

the results beyond these practical limitations we explicitly take advantage of the scaling properties of the fractal clusters [29].

An approximation of the autocorrelation function, equation (13), which is exact up to the first cumulant, can be constructed as

$$g_1(t) = \frac{1}{I(q)} \sum_M N(M)M^2 S(qR_g) \exp(-q^2 D_{eff} t) \tag{14}$$

where the effective diffusion coefficient $D_{eff} = Df(qR_g)$ includes the effects of both translational and rotational diffusion. The function $f(qR_g)$, which reflects the effects of rotational diffusion to the first cumulant, can be derived from equation (13) as

$$f(qR_g) = \frac{D_{eff}}{D} = 1 + \frac{3\sum_l l(l+1)S_l(qR_g)}{4(\beta qR_g)^2 S(qR_g)} \tag{15}$$

and is seen to be a function of qR_g only. Thus, for dynamic light scattering, as for static light scattering, the clusters can be characterised by a single length scale, R_g. At small qR_g, $S_l(qR_g) \simeq 0$ except for $l = 0$, so that $f(qR_g) = 1$, as expected, since the scattered light cannot resolve the anisotropy of the clusters under these conditions. For $qR_g \gg 1$, scaling arguments show [29, 30] that

$$f(qR_g) \simeq 1 + \alpha^2/(4\beta^2) \tag{16}$$

where $\alpha \simeq 1.5$. The shape of $f(qR_g)$ can be calculated using equation (15) with computer-generated clusters. We have calculated $f(qR_g)$ for 20 DLCA clusters each of masses 100, 200, . . . , 900 particles using $\beta = 0.93$ as discussed below. The average value of $f(qR_g)$ is plotted as a function of qR_g in figure 2. As can be seen, the curve approaches 1 when $qR_g < 1$, rises when $qR_g \simeq 1$, and becomes constant again when $qR_g > 5$, as predicted. These results explicitly reflect the consequences of rotational diffusion of an essentially monodisperse distribution on the first cumulant of the autocorrelation function.

We can now evaluate the autocorrelation function for the distribution of DLCA clusters, using equation (14). We use the $f(qR_g)$ shown in figure 2, equation (12) for $S(qR_g)$ and equation (3) for $N(M)$ as appropriate for DLCA clusters. We take $\bar{M} = 165$, as determined from the fit to $I(q)$.

At small angles, where $q\bar{R}_g = qa\bar{M}^{1/d_f}$ is small, rotational diffusion plays almost no role, so that $D_{eff} \simeq D = \zeta/\beta R_g$, and the only unknown parameter in equation (14) is β. Thus we can obtain the experimental value for β for DLCA clusters from a fit of equation

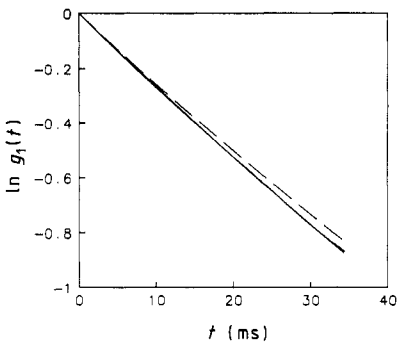

Figure 3. The autocorrelation function measured at $\theta = 15°$ for gold DLCA aggregates. The full curve through the data is a fit using equation (14) and D_{eff}, which includes the effects of rotational diffusion with $\bar{M} = 165$ from the fit to the static light scattering. The fit and the data cannot be distinguished. The broken curve is the same calculation, but excludes the effects of rotational diffusion, which makes only a small contribution since $q\bar{R}_g \simeq 0.75$. A value of $\beta = 0.93$ is obtained from the fit.

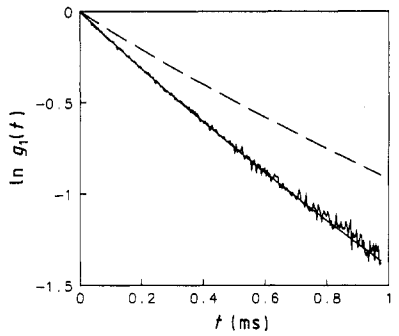

Figure 4. The autocorrelation function measured at $\theta = 96°$ for gold DLCA aggregates. The full curve through the data is a calculation using equation (12) and D_{eff}, which includes the effects of rotational diffusion with $\bar{M} = 165$ from the fit to the static light scattering. The broken curve is the same calculation, but excluding the effects of rotational diffusion, which are significant in this case where $q\bar{R}_g \simeq 4.3$.

(14) to the measured autocorrelation function. This is shown in figure 3 (full curve), where we plot the autocorrelation function measured at $\theta = 15°$, corresponding to $q = 0.0045\ \text{nm}^{-1}$, and $q\bar{R}_g = 0.75$. We obtain $\beta = 0.93$, and the agreement between the fit and the data is so good that the fitted curve cannot be distinguished from the data. The fit includes the effects of rotations, but they play a very small role as can be seen from the broken curve, which is a calculation using $D_{eff} = D$. The value obtained for β is in good agreement with theoretical [31] and computer [32] calculations. We note that a value of $\beta \simeq 1.0$ has been obtained for RLCA clusters, both experimentally [6, 33, 34] and theoretically [31, 32]. The difference for the two regimes is not surprising, given their different fractal dimensions.

At large angles, rotational diffusion is much more important. This is evident in figure 4, where we plot the autocorrelation function measured at $\theta = 96°$, corresponding to $q\bar{R}_g = 4.3$. The autocorrelation function is also calculated, where there are now no unknown parameters. The calculation is in excellent agreement with the data. By contrast, if the effects of rotational diffusion are not included, the calculation deviates considerably from the data as shown by the broken curve in figure 4. Similarly good agreement between the calculation and the data is obtained at all other angles.

We note that we obtain good agreement with the shape of the autocorrelation function over all delay times measured, using the approximate expression, equation (14). This implies that the major contribution to the higher-order cumulants arises from the cluster mass distribution rather than from the effects of rotational diffusion on the shape of the decay of the autocorrelation function of individual clusters.

5. Aggregation kinetics

In the previous section, we investigated the scattering from a single sample with $\bar{R}_g$ comparable to q^{-1}. This enables us to use both static and dynamic light scattering

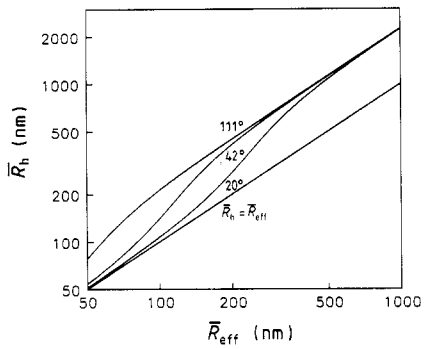

Figure 5. DLCA calibration curves giving the average hydrodynamic radius $\bar{R}_h$ as a function of the effective average radius $\bar{R}_{eff} = \zeta q^2/\Gamma_1$. The curves are for (from the top) $\theta = 111°$, 42° and 20°. The straight line represents $\bar{R}_h = \bar{R}_{eff}$, and hence is for monodisperse spheres without the effects of rotational diffusion.

techniques to study the features of the aggregates, especially the static structure factor and the effects of rotational diffusion. This analysis of the scattering results can be extended to other times during the aggregation, which is essential to draw conclusions about the growth kinetics. Here, we demonstrate how the characteristic cluster size of the distribution can be determined as a function of the aggregation time t_a. However, as we have seen in the previous section, the effects of rotational diffusion cause a significant change in the shape of the autocorrelation function for $q\bar{R}_g > 1$; therefore they also cause a significant change in the apparent average hydrodynamic radius determined from the first cumulant. Thus, we define an *effective* average diffusion coefficient,

$$\bar{D}_{eff} = \frac{\Gamma_1}{q^2} = \frac{\sum_M N(M)M^2 S(qR_g) D_{eff}}{\sum_M N(M)M^2 S(qR_g)}. \tag{17}$$

This is simply an average of the effective diffusion coefficient D_{eff}, weighted by the scattering intensity and the cluster mass distribution. We note that the orientationally averaged static structure factor is used as the intensity weighting. The rotational effects are included in equation (17) only through D_{eff}, which, as expressed in equation (15), is itself an average weighted by the multipoles of $S(qR_g)$.

We can experimentally determine $\bar{D}_{eff}$ from the first cumulant. We note that, in general, $\bar{D}_{eff}$ depends on q due both to the cluster mass distribution and to the contributions of rotational diffusion [26]. Thus the experimentally determined $\bar{R}_{eff} = \zeta/\bar{D}_{eff}$ is also q-dependent. However, since every quantity in equation (17) is known, it is a simple matter to calculate the true average hydrodynamic radius $\bar{R}_h$, which is not q-dependent. This is most conveniently done by means of the DLCA calibration curves in figure 5, where we plot $\bar{R}_h$ as a function of the measured $\bar{R}_{eff}$ at several different angles. For comparison, we also plot the relationship $\bar{R}_h = \bar{R}_{eff}$, representing a monodisperse system with no rotational effects. The shapes of the calibration curves at various angles differ, reflecting the differing onsets of the contribution of rotational diffusion as $q\bar{R}_g$ approaches unity for each value of q. For sufficiently large $\bar{R}_{eff}$ the three calibration curves coincide, as they have all reached the large $q\bar{R}_g$ limit. However, here the difference between $\bar{R}_{eff}$ and $\bar{R}_h$ is pronounced. The additional contribution to the autocorrelation function due to rotational diffusion causes a faster decay; thus if only translational diffusion is considered, the effective average cluster size would be smaller by a factor of about 2 at large qR_g.

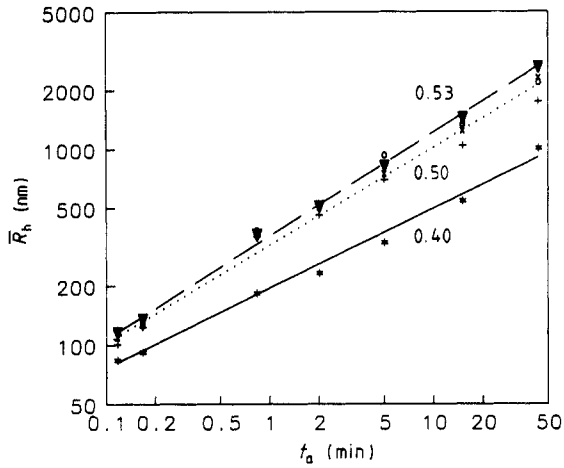

Figure 6. The aggregation kinetics determined by the average hydrodynamic radius $\bar{R}_h$, as a function of the aggregation time t_a. The circles ($\theta = 20°$), crosses ($\theta = 42°$) and pluses ($\theta = 111°$) are obtained using the calibration curves of figure 5. These data give a kinetic exponent of 0.50, shown by the dotted line. The triangles are the values of $\bar{R}_h$, determined from the scaling leading to the master curve. They give a kinetic exponent of 0.53, as shown by the broken line, giving $z = 0.98$. By comparison, the measured $\bar{R}_{eff}$ obtained at $\theta = 42°$ is also plotted using stars. It has a smaller slope, 0.40.

The aggregation kinetics can be obtained from the measurements of the first cumulant at any angle using the appropriate calibration curve. As an example we plot, in figure 6, the values of $\bar{R}_h$ as a function of the aggregation time t_a, determined from experiments performed at several different angles. For comparison we also show by the stars in figure 6 the measured values $\bar{R}_{eff}$ obtained at one of the angles, $\theta = 42°$. The correction provided by the calibration curve due to the effects of rotational diffusion is apparent. The linear behaviour exhibited by the data in the logarithmic plot in figure 6 indicates power-law kinetics. We emphasise, therefore, that the effects of rotational diffusion not only affect the average size of the clusters determined experimentally, but also modify the apparent exponent of the growth kinetics. Thus the full line through the uncorrected data represented by the stars has a slope of 0.40, whereas the corrected hydrodynamic radius grows with an exponent of roughly 0.50 as shown by the dotted line in figure 6.

6. Master curves for dynamic light scattering

In the preceding section we measured the aggregation kinetics using the values that the first cumulant has in the limit as $q \rightarrow 0$. This was accomplished by combining the measured results, obtained at non-zero q, with our knowledge about the cluster mass distribution and about the structure factor. This analysis, therefore, makes use of the calculations to obtain $S(qR_g)$ and various $S_l(qR_g)$ from the computer-generated clusters. There is, however, a considerable amount of additional information in the q dependence of $\bar{D}_{eff}$. In this section we develop a method to scale all of the measured values of $\bar{D}_{eff}$ onto a single master curve, and show that the shape of this master curve reflects many of the features characteristic of diffusion-limited colloid aggregation. This master curve

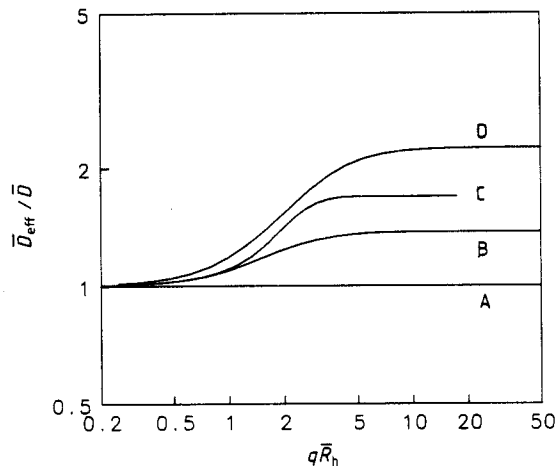

Figure 7. Master curves calculated for different conditions: A, $\bar{D}_{eff} = \bar{D}$, with no polydispersity or rotational diffusion; B, with cluster mass distribution of DLCA, excluding the effects fo rotational diffusion; C, including the effects of rotational diffusion, but with a monodisperse cluster mass distribution; and D, including the effects of both the cluster mass distribution and rotational diffusion for DLCA clusters.

displays the dependence of $\bar{D}_{eff}/\bar{D}$ on the dimensionless quantity $q\bar{R}_h$. Here, $\bar{D} = \zeta/\bar{R}_h$ is the diffusion coefficient that would be determined from the first cumulant at $q = 0$.

Experimentally, only a limited range of q values is accessible so a measurement of the full extent of $\bar{D}_{eff}$ is not possible. However, as the aggregation proceeds, $\bar{M}$ increases and the scattering will be progressively dominated by larger and larger clusters, so that it becomes impossible to extract easily the true hydrodynamic radius $\bar{R}_h$ directly from experiment. We can, however, greatly extend the range over which the q dependence of $\bar{D}_{eff}$ can be measured by exploiting the dynamic scaling of the cluster mass distribution, equation (1). As shown in the appendix, $\bar{D}_{eff}/\bar{D}$ is a function of $q\bar{R}_h$ only; this result reflects the fact that the cluster mass distribution is characterised by $\bar{M}$ and therefore by a single length scale $\bar{R}_h$. This allows us to determine a single master curve for all the data.

To illustrate the significance of the master curve we show how its shape is affected by several key features of the aggregation process in figure 7, where we plot $\bar{D}_{eff}/\bar{D}$, calculated from equation (17) for DLCA clusters, as a function of $q\bar{R}_h$. Curve A is the result for monodisperse spheres so that $\bar{D}_{eff} = \bar{D}$. Without polydispersity and rotational diffusion there is no q dependence. Curve B takes into account the polydispersity as described by the cluster mass distribution $N(M)$ for DLCA, but still ignores rotational effects. This introduces a slight q dependence. In curve C we assume a monodisperse cluster mass distribution, but we use the form for $D_{eff}/D = f(qR_g)$ from equation (15) and figure 2 to include rotational diffusion. Now the q dependence introduced is somewhat greater. Finally, curve D takes account of both $N(M)$ and rotations. This curve exhibits the strongest variation with $q\bar{R}_h$ of all those shown. The shape of the master curve is therefore sensitive to various features characterising the agregation. It depends on the cluster mass distribution and on rotational diffusion, and thus reflects the anisotropies of the clusters. Since $\bar{D}_{eff}/\bar{D}$ is a convolution of $N(M; t_a)$ and $S(qR_g)$ and since $\bar{M}$ increases with increasing aggregation time t_a, the shape of the master curve is also sensitive to the detailed form of the structure factor $S(qR_g)$ in the cross-over region

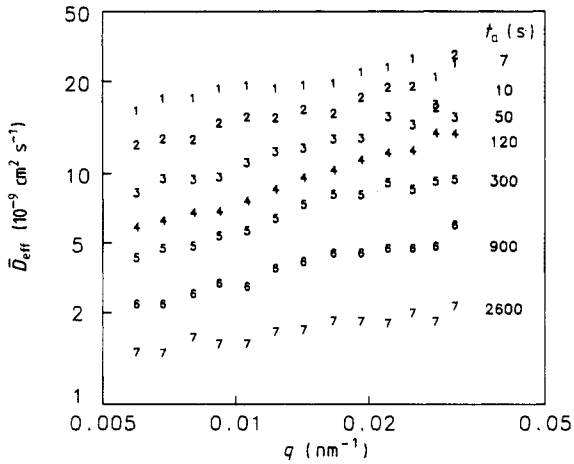

Figure 8. Measured $\bar{D}_{eff}$ as a function of q, taken at different times t_a, as labelled, for colloidal gold.

around $qR_g \simeq 1$. Finally, the scaling factor $\bar{R}_h$ required to shift the data onto the master curve provides the characteristic size of the clusters, and its time dependence will directly reflect the aggregation kinetics.

To produce the master curve from the experimental data, we measure $\bar{D}_{eff}$ as a function of q for several different aggregation times t_a. Using colloidal gold, the aggregation can be halted at t_a to make the measurements. In figure 8, we plot the measured $\bar{D}_{eff}$ as a function of q for samples stopped at seven different values of t_a. With this method, we are able to obtain data at very early stages of the aggregation, despite its rapid rate.

To scale these data onto a single master curve requires a knowledge of $\bar{R}_h$ for each data set. However, to measure $\bar{R}_h$ directly would require data obtained in the $q \to 0$ limit, which is not possible, except at the earliest times. Hence, the scaling factors for the other data sets are obtained empirically by choosing an $\bar{R}_h$, and an equivalent $\bar{D}$, for each data set so that it overlaps with the previous data set. Operationally, this simply involves shifting each data set along the diagonal of the logarithmic plot in figure 8 until they all overlap. With sufficient data, this scaling process is both straightforward and unambiguous. As can be the results shown in figure 9, the data can be scaled to lie on a single master curve. The full curve plotted with the data is the calculation shown in curve D in figure 7, which includes the effects of the cluster mass distribution and rotations. We emphasise that there is no free parameter to scale the calculation with the data. Excellent agreement is found between the calculation and the data for $q\bar{R} < 10$. At higher $q\bar{R}_h$, there is a slight, but persistent, q dependence exhibited by the data, which is absent from the calculation. We speculate that this may be due to internal vibrations of the clusters, which are not included in our calculation. These would be expected to become more important at large $q\bar{R}_h$, and would provide an additional decay mechanism for the autocorrelation function, thereby increasing the measured $\bar{D}_{eff}$. This is consistent with our observation in figure 9.

The scaling factors $\bar{R}_h$ obtained for the data set at each t_a represent an alternative method of determining the aggregation kinetics. We show these values of $\bar{R}_h$ as a function of t_a by the triangles in figure 6. We emphasise that the values of $\bar{R}_h$ determined in this fashion are free of many of the assumptions inherent in the calibration curves used in the previous section. Over most of the aggregation times investigated, very good

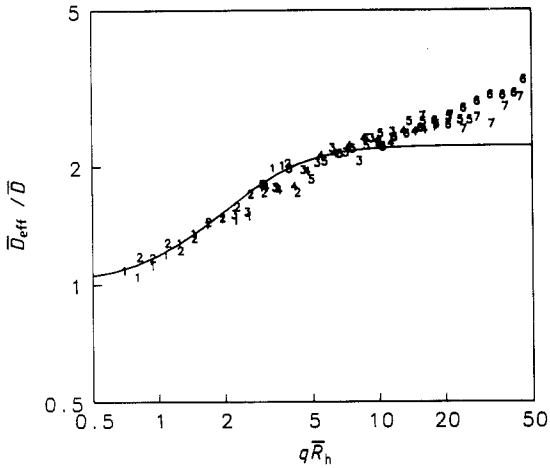

Figure 9. Data from figure 8 scaled onto a master curve, by multiplying each set by a factor of $\bar{R}_h/\zeta$, and plotting as a function of $q\bar{R}_h$. An $\bar{R}_h(t_a)$ is chosen for each data set such that it overlaps with the others. The full curve is the calculated result shown in curve D in figure 7.

agreement is observed by the two methods. However, at the longest times, the $\bar{R}_h$ obtained by the present method increases somewhat more rapidly. This reflects the fact that this method can account for the additional dynamics that are apparent at high $q\bar{R}_h$ in the master curve. Thus the exponent describing the kinetics obtained by this method is again somewhat higher, 0.53 as shown by the broken line in figure 6. This is probably the most accurate method for determining the aggregation kinetics. The large overlapping range of the data sets ensures that the scaling is unambiguous, providing an accurate measure of $\bar{R}_h$. We estimate the fractional uncertainty of $\bar{R}_h$ obtained in this way to be less than 10%. The kinetic exponent for $\bar{R}_h$ is directly related to z. Since $\bar{M} \sim t_a^z$, and since, as we show later, $\bar{R}_g \sim \bar{R}_h$, we have $\bar{R}_h \sim \bar{M}^{1/d_f} \sim t_a^{z/d_f}$. Using the value $d_f = 1.86$ obtained from the static light scattering at later times, we can determine the value of $z = 0.98$, which is in good agreement with the theoretical expectation.

We have previously reported [35] that the effective hydrodynamic radius measured at a single angle, and not corrected for rotational diffusion, increased as t_a^{1/d_f}. This earlier result was incorrect. It was probably obtained using a somewhat aged colloid, and was therefore not truly in the diffusion-limited regime, but was rather in the cross-over between DLCA and RLCA. Nevertheless, despite our earlier error, the essential conclusion of our earlier work, that $z = 1$, remains completely valid, as shown here.

It is clear from the results reported here that a true measure of the dynamic exponent z requires, at the very least, a correction to be made for the effects of rotational diffusion. If this is not done, an incorrect result for z is obtained. In a recent paper, Wilcoxon *et al* [36] studied the aggregation kinetics of colloidal gold using dynamic light scattering, and obtained a value of $z/d_f \simeq 0.4$ from the time dependence of $\bar{R}_{eff}$, consistent with our results reported here. However, they did not make any corrections for rotational diffusion, and thus misinterpreted their measurements, arriving at incorrect conclusions concerning the kinetics of DLCA for colloidal gold. If they had properly included the consequences of rotational diffusion, they would presumably have determined a value of $z \simeq 1$, in accord with our measurements, and as expected theoretically.

7. Universal behaviour of DLCA

The procedure used in the previous section to obtain the master curve is based on the scaling properties of the cluster mass distribution and the structure factor. This scaling

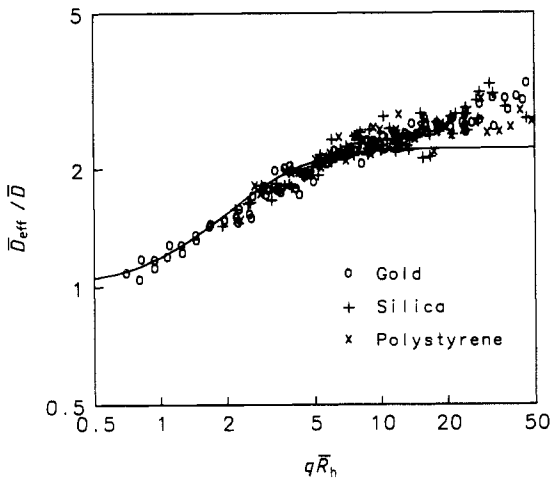

Figure 10. Master curves for gold (○), silica (+) and polystyrene (×) for DLCA. The full curve is the calculated result shown in curve D in figure 7. The master curves for each colloid are indistinguishable.

procedure has the desirable feature that all properties, specific to the colloid used, drop out. As we have shown, the shape of the master curve is very sensitive to several key features characteristic of the aggregation process. Thus this provides a method to compare critically the behaviour of different colloid systems, and to test the universality of diffusion-limited colloid aggregation. In addition, static light scattering can provide an additional measure of the universality through the determination of the fractal dimension and the structure factor of the clusters.

To test this universality of DLCA, we choose, in addition to the gold system, two very different colloids: silica and polystyrene latex. Each of these three colloids comprises a different material; each colloid is stabilised by different functional groups; the aggregation of each colloid is initiated by a different method; each colloid forms completely different interparticle bonds upon aggregation. However, each of them can be aggregated in either the diffusion-limited or reaction-limited regime.

Unlike the gold, we do not have a suitable method for stopping the aggregation of the other two colloids. Instead, all the data for these two colloids were taken repeatedly as a function of q by changing the angle of the detector while the aggregation proceeded. Since we require sets of data obtained at the same value of t_a and therefore the same value of $\bar{M}$, the first cumulants at each angle were interpolated, assuming power-law kinetics, to obtain sets of $\bar{D}_{eff}$ at the same t_a, similar to those shown in figure 8 for gold. The master curves for the other two colloids were then independently obtained following the same procedures described in the previous section. The kinetics were determined from the time dependence of the scaling parameter $\bar{R}_h$. In addition, the static light scattering intensity was measured concurrently, allowing the fractal dimensions to be determined independently.

In figure 10, we plot the three master curves obtained independently from the different colloids. We emphasise that there are no adjustable parameters in their comparison. Nevertheless, the master curves for each of the colloids are indistinguishable. Furthermore, the same agreement between the calculated master curve and the data is obtained. In addition, the behaviour of the static scattering from each of the colloids is the same, as shown in figure 11. The measured fractal dimensions were $d_f = 1.86$ to within ± 0.01, for each case, as shown in table 1. Finally, the growth kinetics of each

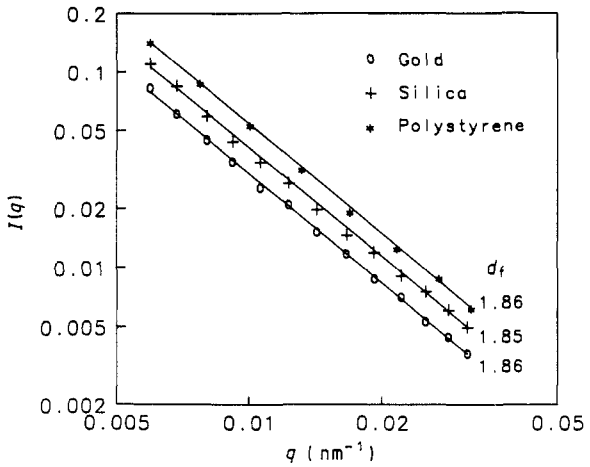

Figure 11. Static light scattering from DLCA aggregates of gold (○), silica (+) and polystyrene (*). The measured fractal dimensions are: gold, $d_f = 1.86$; silica, $d_f = 1.85$; and polystyrene, $d_f = 1.86$, and are identical to within experimental error.

Table 1. Comparison of quantities for the three colloids.

			Dynamic prefactor (nm/min$^{0.54}$)	
Colloid	d_f	z	$1.44a/t_0^{0.54}$	Measured
Gold	1.86	0.98	454	365
Silica	1.85	1.00	272	166
Polystyrene	1.86	1.05	128	115

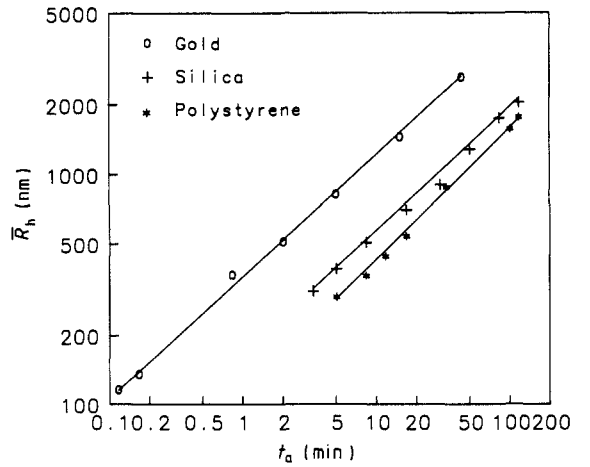

Figure 12. Kinetics of DLCA aggregation for gold (○), silica (+) and polystyrene (*), plotted on a logarithmic scale. The slopes for the straight lines are: 0.53 for gold, giving $z = 0.98$; 0.54 for silica, giving $z = 1.00$; and 0.56 for polystyrene, giving $z = 1.05$.

colloid also had the same behaviour, as shown in figure 12, where the values of $\bar{R}_h$, obtained from the scaling, are plotted as a function of aggregation time t_a, for the three colloids. They all exhibit linear behaviour in the logarithmic plot. From the slope of each curve and the measured fractal dimension, we can determine the kinetic exponent z for

each colloid. As listed in table 1, the values of z thus obtained are all nearly unity, in agreement with the theoretical prediction, $z = 1$.

A further quantitative check of the validity of the theory is obtained from the value of the prefactor of the power-law kinetics for each colloid, determined from the plot. Theoretically, from equation (4*a*) at long times, we have

$$\bar{R}_g \simeq a(t_a/t_0)^{1/d_f} \tag{18}$$

where t_0 is given by equation (4*b*). This must be expressed in terms of $\bar{R}_h$, which is determined from the scaling to produce the master curves. To do so, we define the nth moment of the distribution as

$$X_n = \sum N(M)M^n. \tag{19}$$

We can then express both average radii, $\bar{R}_g$ and $\bar{R}_h$, in terms of the appropriate moments,

$$\bar{R}_g = a(X_1/X_0)^{1/d_f}$$

$$\bar{R}_h = a\beta X_2/X_{2-1/d_f}.$$

Evaluating these expressions, using the DLCA cluster mass distribution, equation (3), we find that

$$\bar{R}_h = \frac{2\beta}{\Gamma(3-1/d_f)}\bar{R}_g \simeq 1.44\bar{R}_g$$

where $\Gamma(\nu)$ is the gamma function. Therefore, we have

$$\bar{R}_h = 1.44a(t_a/t_0)^{1/d_f} \tag{20}$$

so that the calculated prefactor is $1.44a/t_0^{1/d_f}$. The calculated and measured values for each colloid are compared in table 1. Again we find remarkable agreement in each case, considering all the approximations we have made and the experimental uncertainties.

In this section, we have compared the behaviour of three completely different colloids aggregated by DLCA. We find that the shapes of the master curves, determined independently from the dynamic light scattering data from each colloid, are identical. Furthermore the fractal dimension of the clusters for each colloid, determined from the static light scattering, as identical. Finally, the aggregation kinetics for each colloid, determined from the scaling procedure used to form the master curves, all exhibit a power-law dependence, with identical dynamic exponents. In addition, the prefactors of these power-law kinetics agree quantitatively with theoretical predictions. These observations are convincing evidence of the universality of diffusion-limited colloid aggregation.

8. Conclusions

In this paper, the process of colloid aggregation in the diffusion-limited regime is studied using both static and dynamic light scattering. We show that the combination of both scattering techniques provides an excellent probe of the aggregation process. Many of the important features can be determined: the fractal dimension of the clusters; the structure factor of the clusters; the cluster anisotropy as reflected in the rotational diffusion; the cluster mass distribution; and the aggregation kinetics. We present a

detailed description of static and dynamic light scattering from colloidal aggregates, which is in good agreement with the experimental results. Static light scattering, with $q\bar{R}_g \gg 1$, is used to measure the fractal dimension; when $q\bar{R}_g \simeq 1$ it is used to measure the cross-over behaviour of the structure factor due to the finite extent of the aggregates. Dynamic light scattering is used to determine the shape of the cluster mass distribution and the effects of rotational diffusion of the aggregates when $q\bar{R}_g > 1$. When the effects of rotational diffusion are properly included, dynamic light scattering can be used to obtain a measure of the true size of the characteristic cluster. We have also measured the ratio of the hydrodynamic radius to the radius of gyration of individual clusters, and find $\beta = 0.93$ for DLCA aggregates.

A method is developed to scale the results of dynamic light scattering onto a single master curve. The sensitivity of dynamic light scattering to the key features of the aggregation process is reflected in the shape of this master curve. Since the master curves are independent of the specifics of the colloid system, they can be used to test critically the universality of DLCA. This universality is confirmed by showing that the master curves obtained independently from three completely different colloids are identical. In addition, static light scattering measurements of the fractal dimension and dynamic light scattering measurements of the aggregation kinetics are also identical for the three colloids. These results provide convincing evidence that diffusion-limited colloid aggregation is a universal kinetic growth process.

Appendix

Here we prove that the ratio of the average effective diffusion coefficient and its value at $q = 0$, $\bar{D}_{\text{eff}}/\bar{D}$, is a function of $q\bar{R}_h$ only.

We name $F(q, \bar{R}_h) = \bar{D}_{\text{eff}}/\bar{D}$, where $\bar{R}_h = \zeta/\bar{D}$. Also $D_{\text{eff}}/D = f(qR_g)$, which is a function of qR_g only, as shown in equation (15). Since $\bar{D}_{\text{eff}} = \Gamma_1/q^2$, according to equation (17),

$$F(q, \bar{R}_h) = \frac{\sum_M N(M)M^2 S(qR_g)D_{\text{eff}}/\bar{D}}{\sum_M N(M)M^2 S(qR_g)}. \tag{A1}$$

Defining $R_g/\bar{R}_h = r$, $M/\bar{M}' = m$, where $\bar{M}' = (\bar{R}_h/a)^{d_f}$ is a moment of the cluster mass distribution, and consequently, $m = r^{d_f}$. We also name $q\bar{R}_h = x$. Recall from equation (1) that we have

$$N(M)M^2 = \psi(m)m^2. \tag{A2}$$

We now convert the summation $\Sigma_M N(M)$ to an integral, $\int N(M)\,\mathrm{d}M$, and rewrite equation (A1) as

$$F(q, \bar{R}_h) = \int \mathrm{d}m\, \psi(m)m,^2 S(xr)f(xr)/(\beta r) \Big/ \int \mathrm{d}m\, \psi(m)m^2 S(xr) \tag{A3}$$

$$= \int \mathrm{d}r\, r^{3d_f}\psi(r^{d_f})S(xr)f(xr) \Big/ \beta \int \mathrm{d}r\, r^{3d_f-1}\psi(r^{d_f})S(xr). \tag{A4}$$

It is clear from equation (A4) that $F(q, \bar{R}_h) = F(x)$, that is, it is a function of $q\bar{R}_h$

only. Hence, the quantity $\bar{D}_{\text{eff}}/\bar{D}$ scales with $q\bar{R}_{\text{h}}$, which assures the existence of the master scaling curve.

References

[1] Meakin P 1988 *Phase Transitions and Critical Phenomena* vol 12, ed C Domb and J L Liebowitz (New York: Academic) p 335
[2] Weitz D A and Huang J S 1984 *Kinetics of Aggregation and Gelation* ed F Family and D P Landau (Amsterdam: North-Holland)
[3] Weitz D A, Huang J S, Lin M Y and Sung J 1985 *Phys. Rev. Lett.* **54** 1416
[4] Verway E J W and Overbeek J T G 1948 *Theory of the Stability of Lyophobic Colloids* (Amsterdam: Elsevier)
[5] Weitz D A, Lin M Y and Huang J S 1987 *Physics of Complex and Supermolecular Fluids* ed S A Safran and N A Clark (New York: Wiley) p 509
[6] Lin M Y, Lindsay H M, Weitz D A, Ball R C, Klein R and Meakin P 1990 *Phys. Rev.* A **41** 2005
[7] Lin M Y, Lindsay H M, Weitz D A, Ball R C, Klein R and Meakin P 1989 *Proc. R. Soc.* A **423** 71
[8] Lin M Y, Lindsay H M, Weitz D A, Ball R C, Klein R and Meakin P 1989 *Nature* **339** 360
[9] Meakin P 1983 *Phys. Rev. Lett.* **51** 1119
[10] Kolb M, Botet R and Jullien R 1983 *Phys. Rev. Lett.* **51** 1123
[11] Weitz D A and Oliveria M 1984 *Phys. Rev. Lett.* **52** 1433
[12] Aubert C and Cannell D S 1986 *Phys. Rev. Lett.* **56** 738
[13] Matsushita M, Hayakawa Y, Sumida K and Sawada Y 1986 *Proc. First Int. Conf. for Science on Form* ed S Ishizaka (Tokyo: KTK Scientific) p 23
[14] Dimon P, Sinha S K, Weitz D A, Safinya C R, Smith G S, Varady W A and Lindsay H M 1986 *Phys. Rev. Lett.* **57** 595
[15] Vicsek T and Family F 1984 *Phys. Rev. Lett.* **52** 1669
[16] Cohen R J and Benedek G B 1982 *J. Chem. Phys.* **86** 3696
[17] Meakin P, Vicsek T and Family F 1985 *Phys. Rev.* B **31** 564
[18] Weitz D A and Lin M Y 1986 *Phys. Rev. Lett.* **57** 2037
[19] Pefferkorn E, Pichot C and Varoqui R 1988 *J. Physique* **49** 983
[20] Turkevich J, Stevenson P C and Hiller J 1951 *Faraday Soc. Disc.* **11** 55
[21] Enustun B V and Turkevich J 1963 *J. Am. Chem. Soc.* **85** 3317
[22] Lin M Y, Klein R, Lindsay H M, Weitz D A, Ball R C and Meakin P 1990 *J. Colloid Interface Sci.* to appear
[23] Lindsay H M, Lin M Y, Weitz D A, Sheng P, Chen Z, Klein R and Meakin P 1987 *Faraday Disc. Chem. Soc.* **83** 153
[24] Olivier B J and Sorenson C M 1990 *Phys. Rev.* A **41** 2093
[25] Berne B J and Pecora R 1976 *Dynamic Light Scattering* (New York: Wiley)
[26] Lindsay H M, Klein R, Weitz D A, Lin M Y and Meakin P 1988 *Phys. Rev.* A **38** 2614
[27] Pusey P N 1976 *Photon Correlation and Velocimetry* ed H Z Cummins and E R Pike (New York: Plenum) p 45
[28] Sheu E Y, Chen S H and Huang J S 1987 *J. Phys. Chem.* **91** 1535
[29] Lindsay H M, Klein R, Weitz D A, Lin M Y and Meakin P 1989 *Phys. Rev.* A **39** 3112
[30] Lindsay H M, Lin M Y, Weitz D A, Ball R C, Klein R and Meakin P 1988 *Proc. Photon Correlation Techniques and Applications* vol 1, ed J B Abbiss and A E Smart (Washington: OSA) p 122
[31] Hess W, Frisch H L and Klein R 1986 *Z. Phys.* B **64** 65
In equation (14) of this paper, the 4 should be replaced by 2.
[32] Chen Z-Y, Meakin P and Deutch J M 1987 *Phys. Rev. Lett.* **59** 2121; Meakin P, Chen Z-Y and Deutch J M 1984 *J. Chem. Phys.* **82** 3786
[33] Wiltzius P 1987 *Phys. Rev. Lett.* **58** 710
[34] Wiltzius P and van Saarloos W 1987 *Phys. Rev. Lett.* **59** 2123
[35] Weitz D A, Huang J S, Lin M Y and Sung J 1984 *Phys. Rev. Lett.* **53** 1651
[36] Wilcoxon J P, Martin J E and Schaefer D W 1989 *Phys. Rev.* A **39** 2675

J. Phys.: Condens. Matter **2** (1990) 5283. Printed in the UK

ERRATUM

Universal diffusion-limited colloid aggregation by M Y Lin, H M Lindsay, D A Weitz, R Klein, R C Ball and P Meakin (*J. Phys.: Condens. Matter* 1990 **13** 3093–3113)

Page 3107

The data in figure 8 were inadvertently substituted with a different set of data in the preparation of the figure with our computer graphics routine. A figure with the correct data is shown here. The correct data were used in the scaling plots, figures 9 and 10, of the original paper. We thank a colleague at Sandia for pointing out this error.

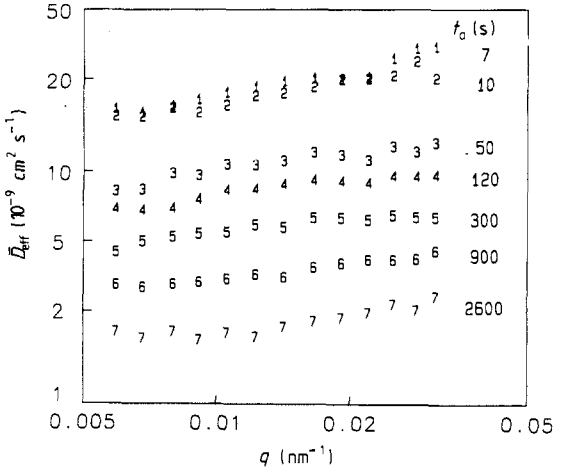

0953-8984/90/235283 + 01 $03.50